Molecular Biology of the Cell
Vol. 20, 2593–2604, May 15, 2009

ERp29 Restricts Connexin43 Oligomerization in the Endoplasmic Reticulum

Shamie Das,*† Tekla D. Smith,*† Jayasri Das Sarma,‡ Jeffrey D. Ritzenthaler,* Jose Maza,* Benjamin E. Kaplan,* Leslie A. Cunningham,* Laurence Suaud,§ Michael J. Hubbard,‖ Ronald C. Rubenstein,§ and Michael Koval*¶

*Department of Medicine, Division of Pulmonary, Allergy and Critical Care Medicine and ¶Department of Cell Biology, Emory University School of Medicine, Atlanta GA 30322; ‡Neuroscience Group, Indian Institute of Science Education and Research, Kolkata, India 700106; §Division of Pulmonary Medicine, Children's Hospital of Philadelphia, and Department of Pediatrics, University of Pennsylvania School of Medicine, Philadelphia, PA 19104; and ‖Department of Paediatrics, University of Melbourne, Melbourne, Victoria 3052, Australia

Submitted August 1, 2008; Revised March 12, 2009; Accepted March 13, 2009
Monitoring Editor: Jeffrey L. Brodsky

Connexin43 (Cx43) is a gap junction protein that forms multimeric channels that enable intercellular communication through the direct transfer of signals and metabolites. Although most multimeric protein complexes form in the endoplasmic reticulum (ER), Cx43 seems to exit from the ER as monomers and subsequently oligomerizes in the Golgi complex. This suggests that one or more protein chaperones inhibit premature Cx43 oligomerization in the ER. Here, we provide evidence that an ER-localized, 29-kDa thioredoxin-family protein (ERp29) regulates Cx43 trafficking and function. Interfering with ERp29 function destabilized monomeric Cx43 oligomerization in the ER, caused increased Cx43 accumulation in the Golgi apparatus, reduced transport of Cx43 to the plasma membrane, and inhibited gap junctional communication. ERp29 also formed a specific complex with monomeric Cx43. Together, this supports a new role for ERp29 as a chaperone that helps stabilize monomeric Cx43 to enable oligomerization to occur in the Golgi apparatus.

INTRODUCTION

Connexins form gap junction channels that mediate intercellular communication by allowing the direct transfer of ions and small aqueous molecules between neighboring cells or by serving as hemichannels at the plasma membrane (Harris, 2001; Goodenough and Paul, 2003; Saez *et al*., 2003; Laird, 2006). There are >20 human connexin genes and one of the most ubiquitously expressed is connexin43 (Cx43). Several diseases have been linked to mutations in different connexin genes, including Cx43 (Kelsell *et al*., 2001; Laird, 2008). Many of these mutant connexins are not efficiently processed and lack the ability to form functional gap junction channels. Determining how mutant connexins are mistargeted requires a more complete understanding of how normal connexins are processed by the cell.

A gap junction hemichannel consists of six connexins, which oligomerize before delivery to the plasma membrane (Martin and Evans, 2004; Segretain and Falk, 2004; Koval, 2006). Unlike most multimeric membrane channels, Cx43 is unusual in that it does not oligomerize in the endoplasmic reticulum (ER) (Musil and Goodenough, 1993), which is more commonly a prerequisite to further transport along the secretory pathway (Ellgaard and Helenius, 2003; Anelli and Sitia, 2008). Instead, Cx43 is transported out of the ER as an apparent monomer that then oligomerizes in the Golgi complex (Musil and Goodenough, 1993; Koval *et al*., 1997). Although other connexins, such as Cx46 (Koval *et al*., 1997), also oligomerize in the Golgi apparatus, this is not a universal pathway for connexin oligomerization because other gap junction proteins, such as Cx32, preferentially oligomerize in the ER (Martin and Evans, 2004; Koval, 2006). Understanding the molecular basis for this difference, as well as the ability of monomeric Cx43 to be transported from the ER to the Golgi apparatus has proven difficult, because little is known about chaperones that regulate connexin folding. In particular, it seemed likely that one or more chaperones would be required to stabilize Cx43 as monomers in the ER and the early secretory pathway.

One clue to a putative Cx43 chaperone came from previous studies using 4-phenylbutyrate (4-PBA), a histone deacetylase inhibitor that influences the expression and function of several proteins, including heat shock proteins and connexins (Rubenstein and Zeitlin, 2000; Berthoud *et al*., 2003; Asklund *et al*., 2004; Wright *et al*., 2004; Khan *et al*., 2007). Importantly, 4-PBA improves the trafficking of several mutant transmembrane proteins, including the ΔF508 mutant of cystic fibrosis transmembrane regulator (CFTR) (Rubenstein *et al*., 1997). We found that 4-PBA enhanced the ability of HeLa cells to process overexpressed Cx43 that would otherwise saturate the quality control pathway in these cells (Das Sarma *et al*., 2005; Das Sarma *et al*., 2008). Because 4-PBA alters protein expression, these observations suggested that the ability of 4-PBA to compensate for Cx43 overexpression was because of the increased

This article was published online ahead of print in *MBC in Press* (http://www.molbiolcell.org/cgi/doi/10.1091/mbc.E08–07–0790) on March 25, 2009.

† These authors contributed equally to this work.

Address correspondence to: Michael Koval (mhkoval@emory.edu).

expression of one or more elements of the connexin quality control pathway.

The effect of 4-PBA on improving the folding and secretion of ΔF508-CFTR is mediated through a widely expressed ER-associated chaperone known as ERp29 (Suaud *et al*., 2008). ERp29 has also been shown to promote the folding and secretion of thyroglobulin (Sargsyan *et al*., 2002; Baryshev *et al*., 2006) and the *Drosophila* paralogue of ERp29, Windbeutel, is required for transport of heparan sulfate 2-*O*-sulfotransferase (Pipe) from the ER to the Golgi apparatus (Ma *et al*., 2003). ERp29 also facilitates the unfolding and ER retrotranslocation of the polyomavirus VP1 protein, a key step in the virus infection cycle (Magnuson *et al*., 2005; Rainey-Barger *et al*., 2007).

The emerging role for ERp29 in regulating protein trafficking suggests the possibility of an analogous role for ERp29 in regulating Cx43 transport along the secretory pathway. Here, we provide evidence that ERp29 stabilizes monomeric Cx43 in the ER and that interference with ERp29 expression inhibited Cx43 secretion and decreased the efficiency of gap junction formation by Cx43. By contrast, interference with ERp29 expression had little effect on Cx32, underscoring a role for ERp29 as a chaperone that can distinguish between different classes of connexins. The ability of ERp29 to regulate Cx43 provides a mechanistic framework for understanding how Cx43 oligomerization into hexamers can occur in after exit from the ER.

MATERIALS AND METHODS

Antibodies and Reagents

Rabbit anti-Cx43 (Civitelli *et al*., 1993) was generated using 6 His-tagged C-terminal tail constructs as described previously. Rabbit anti-ERp29 was prepared as described previously (Hubbard and McHugh, 2000) and also purchased from Affinity Bioreagents (Golden, CO); both antibodies gave equivalent results. Anti-protein disulfide isomerase A1 (PDI) was from Sigma-Aldrich (St. Louis, MO). Monoclonal anti-Cx43 was from Millipore Bioscience Research Reagents (Temecula, CA). Fluorescent and horseradish peroxidase-conjugated secondary antibodies and streptavidin were from Jackson ImmunoResearch Laboratories (West Grove, PA). Anti-enhanced green fluorescent protein (EGFP) was from Clontech (Mountain View, CA). BioMag particles coated with goat anti-mouse immunoglobulin G (IgG) were from Polysciences (Warrington, PA). Triton X-100 was from Roche Molecular Biochemicals (Indianapolis, IN). Unless otherwise specified, all other reagents were from Sigma-Aldrich.

Cell Culture

Stably transfected HeLa cells were prepared as described previously (Maza *et al*., 2003; Daugherty *et al*., 2007) and cultured in minimal essential medium containing Earle's salts, L-glutamine, 10% heat-inactivated bovine calf serum, 100 IU/ml penicillin, 100 μg/ml streptomycin, and 0.5 mg/ml Geneticin (G-418; Invitrogen, Carlsbad, CA). Rat osteoblastic (ROS) 17/2.8, NIH 3T3, and A549 cells were cultured as described previously (Das Sarma *et al*., 2001; Wang *et al*., 2003).

Immunofluorescence

For immunofluorescence, cells cultured on glass coverslips were fixed and permeabilized with MeOH:acetone (1:1) and then washed three times with phosphate-buffered saline (PBS), followed by PBS + 0.5% Triton X-100 and PBS + 0.5% Triton X-100 + 2% goat serum (PBS/GS). The cells were incubated with primary antibodies diluted into PBS/GS for 1 h, washed, and then labeled with secondary antibodies diluted into PBS/GS. The cells were then washed with PBS, mounted into MOWIOL, and visualized by fluorescence microscopy using an X-70 microscope system (Olympus, Tokyo, Japan) with an Orca-1 charge-coupled device camera (Hamamatsu, Bridgewater, NJ), and Image-Pro image analysis software (MediaCybernetics, Bethesda, MD). Morphometric analysis of immunofluorescence images for gap junction plaque formation was done by scoring regions localized to cell–cell contact interfaces with area >6 μm^2 and mean fluorescence intensity of ≥128 (50% max). Data were from three independent immunofluorescence preparations, scoring data from at least five fields per preparation. Each field contained roughly 20 cells (0.07 mm^2/field). For colocalization with EGFP-tagged ERp29, anti-EGFP and Cy2-labeled goat anti-rabbit IgG was used because the endogenous EGFP fluorescence was low but sufficiently visible to be used for imaging live cells at high gain for microinjection experiments.

Constructs, RNA Interference, and Transfection

Human ERp29 cDNA was obtained by reverse transcription of HeLa cell RNA and confirmed by sequencing. Tagged ERp29 constructs were produced by polymerase chain reaction (PCR) amplification in a Robocycler (Stratagene, La Jolla, CA) by using High Fidelity DNA polymerase (Roche Molecular Biochemicals), starting with ERp29 cDNA as a template. The ERp29 signal sequence was amplified using 5′-CGGCTAGCCG GCGATATGGC TGCCGCTG-3′ and 5′-GCACCGGTTT GGTGTGCAGG CCGCTGCC-3′ as sense and antisense primers. The resulting PCR product was cut with NheI and AgeI, and ligated into a doubly cut pEGFP-C3 (Clontech) to produce ERp29 signal-EGFP, which was transformed into bacterial stocks. The remainder of the ERp29 sequence was amplified using 5′-CGAAGCTTGC AGCACTGCAC ACCAAGGGCG CCCTTCCCCT GGA-3′ and 5′-CCCGGATCCT TACAGCTCCT CTTTCTCGGC CC-3′ as sense and antisense primers. The resulting PCR product was cut with HindIII and BamHI and ligated into doubly cut plasmids containing ERp29 signal-EGFP to produce EGFP-ERp29 (Supplemental Figure S1). A putative dominant-negative EGFP-ERp29 construct (Magnuson *et al*., 2005; Barak *et al*., 2009; Rainey-Barger *et al*., 2009) containing the N-terminal domain of EGFP-ERp29 and the KEEL ER retention sequence (EGFP-ERp29-N) was produced by amplifying EGFP-ERp29 with 5′-GGTACCATGG CTGCCGCTGT GCCCCG-3′ and 5′-TCTAGATTAC AGCTCCTCTT TCATACCTAG GTAGACCCCT T-3′ as sense and antisense primers. The resulting PCR product was cut with KpnI and XbaI and ligated into doubly cut pcDNA3.1 (Clontech). DNA for transfection was purified from bacteria using the Maxiprep kit (QIAGEN, Valencia, CA) according to the manufacturer's instructions. Before transfection, cDNA was purified by ethanol precipitation. HeLa cells were transiently transfected with either EGFP-ERp29 or EGFP-ERp29-N by using Lipofectamine (Invitrogen) and analyzed 2 d after transfection. Transfection efficiencies using this approach were typically >70% as assessed by scoring cells by fluorescence microscopy.

Predesigned, preannealed, double-stranded small interfering RNA (siRNA) oligonucleotides (oligos) to human ERp29 [gene ID: 190546, oligos 18717 (h1) and s21576(h2)], rat ERp29 [gene ID: 117030, oligos 190547 (r1) and s138452 (r2)] and control oligonucleotides (4635) were from Ambion (Foster City, CA). Unless otherwise indicated, experiments were done using h1 (for human cells) or r1 (for rat cells). In some cases, siRNAs were labeled with Cy3 using the Ambion Silencer labeling kit according to the manufacturer's instructions. Before siRNA treatment, cells were incubated overnight in Opti-MEM (Invitrogen) + 4% fetal bovine serum without antibiotics and then changed to serum-free Opti-MEM. Double-stranded siRNA oligos were diluted in serum-free Opti-MEM medium using a 1:20 ratio of Oligofectamine (Invitrogen) to siRNA (microliters:picomoles) and at a final siRNA concentration of 1 pmol/μl. For 35-mm dishes, 90 pmol/dish of siRNA was added; 60-mm dishes were treated with 175 pmol/dish. Cells were analyzed by immunofluorescence, dye transfer, or immunoblot 2 d after addition of siRNA.

Quantitative Reverse Transcription (RT)-PCR

PCR primers corresponding to Cx43 (sense, TTGCTGCTGG ACATGAACTC; antisense, CAAGCCGGTT TAAATCTCCA; product size, 119 base pairs) and 18s RNA (sense, GGACCAGAGC GAAAGCA; antisense, ACCCACGGAA TCGAGAAA; product size, 337 base pairs) were obtained from Sigma-Aldrich. RNA was isolated from untreated and treated cells with TRIzol reagent (Invitrogen), treated with DNase (Promega, Madison, WI) to remove contaminating genomic DNA, and then converted to cDNA with reverse transcriptase and a mix of random hexamer and oligo(dT) primers (Invitrogen). The resulting cDNAs were amplified by real-time quantitative PCR using the LightCycler-FastStart DNA Master SYBR Green I kit in the Cepheid SmartCycler real-time PCR cycler (Molecular Devices, Sunnyvale, CA). The cycling conditions were as follows: initial denaturation at 95°C for 10 min, followed by 40 cycles at 95°C for 15 s, 60°C for 10 s, and 72°C for 10 s. Relative amounts of PCR product were calculated using the comparative C(T) method (Schmittgen *et al*., 2008). Experiments were performed in triplicate for each data point, and negative controls without templates and that were not amplified by reverse transcriptase were included in the analysis. The size of the PCR products amplified by real-time PCR was confirmed by agarose gel electrophoresis analysis.

Protein Analysis

Postnuclear homogenates were prepared with a ball-bearing homogenizer and centrifugation as described previously (Koval *et al*., 1995, 1997; Das Sarma *et al*., 2002). Samples were added to 2× sample buffer containing 50 mM dithiothreitol (DTT), resolved by SDS-polyacrylamide gel electrophoresis (PAGE), transferred to Immobilon membranes (Millipore, Billerica, MA), and blotted using antibodies described above. Specific signals corresponding to a given protein were detected by immunoblot using enhanced chemiluminescence (ECL) reagent (GE Healthcare, Pittsburgh, PA) and quantified with an EDAS system (Eastman Kodak, Rochester, NY). Normalization for protein content was done using parallel samples analyzed for actin. Statistical significance was determined by *t* test. For proteasome inhibitor experiments, cells were incubated for 4 h with 10 μM lactacystin before harvest and biochemical analysis (Qin *et al*., 2003). For coimmunopurification, cells were solubilized in PBS containing 0.1% Triton X-100 and then incubated overnight at 4°C with

BioMag goat anti-mouse IgG-coated particles (Polysciences) precoated with mouse anti-Cx43 IgG, 0.25% bovine serum albumin, and 0.2% gelatin. The magnetic particles were isolated using a ceramic magnet (Stratagene), washed with PBS at 4°C, resuspended in SDS-PAGE sample buffer containing DTT, and then analyzed by immunoblot.

To measure Cx43 turnover, HeLa/Cx43 cells treated with either control or ERp29 siRNA were incubated in Met/Cys-free medium for 1 h and then labeled with medium containing 5 μCi/ml ^{35}S-EasyTag (PerkinElmer Life and Analytical Sciences, Boston, MA) for 2 h at 37°C. The cells were then washed and chased for varying amounts of time in normal medium washed, harvested, and then solubilized in 1% Triton X-100 + 0.1% SDS. Magnetic goat anti-rabbit IgG-coated particles were incubated for 2 h with rabbit anti-Cx43 in PBS containing 0.25% bovine serum albumin and 0.2% gelatin. The particles were then added to the solubilized cells and incubated for 2 h at 4°C. The magnetic particles were then magnetically immunoisolated and resolved by SDS-PAGE as described above. Samples were transferred to Immobilon membranes and detected by autoradiography. Half-times ($t_{1/2}$) were calculated from exponential decay curve that were fit to the data using Excel (Microsoft, Redmond, WA).

Blue Native (BN) Gel Electrophoresis

Nondenaturing blue native gel electrophoresis was done using a method based on Wittig *et al*. (2006). Samples were either untreated, treated for 5 h with 6 μg/ml brefeldin A (BFA), or treated with siRNA as described above. The samples were homogenized, and postnuclear supernatants were diluted into BN sample buffer (50 mg/ml Serva G [Coomassie Blue, G250] and 30% glycerol in double distilled H_2O). Blue native gels consisted of a 4.2% polyacrylamide stacking gel on a 7.5% resolving gel in Bis Tris-HCl, pH 7.0. Five microliters of each sample was loaded/lane, and the gels were run using 50 mM Tricine/15 mM Bis Tris, pH 7.0, cathode buffer containing 0.01% Serva G and 50 mM Bis Tris-HCl, pH 7.0, on ice. The gels were run at constant voltage (100 V) on ice for 3–6 h until the blue dye migrated approximately two thirds of the way along the resolving gel. Cathode buffer was replaced with dye-free cathode buffer, and the gel was run to completion at 150-V constant voltage for 2 h. Gels were removed and incubated in transfer buffer [50 mM Tris, 380 mM glycine, 0.025% (wt/vol) SDS, and 20% MeOH] for 30 min at room temperature, and proteins were transferred to Immobilon P by using a semi-dry apparatus (Bio-Rad). The blots were processed using a standard immunoblot protocol, using appropriate primary antibodies, horseradish peroxidase-conjugated goat anti-rabbit IgG as a secondary antibody, and ECL for detection. Lanes were scanned and analyzed using Image-Pro software (MediaCybernetics).

Microinjection

Cells cultured on glass coverslips were used for microinjection. A glass micropipette containing 2 mg/ml calcein or 10 nM Alexa Fluor588 (Alexa588) in 200 mM KCl (Invitrogen) was used to microinject a single cell in a field, and the diffusion of calcein or Alexa588 by gap junctional intercellular communication was assessed as the number of cells containing fluorescent dye after a 3-min incubation period (Koval *et al*., 1995). A cell was scored as positive if it had a representative area with an average fluorescence intensity of at least 10% of the microinjected cell fluorescence intensity as determined with Image-Pro. Typically, the extent of dye transfer after prolonged incubation (>15 min) did not increase by more than an additional 20% (Koval *et al*., 1995). Statistical significance was calculated using the Mann–Whitney *U* test. Note that the intercellular transfer of Alexa568 through Cx43 channels by control cells was less efficient than calcein, which is a smaller molecule, consistent with previous reports (Koval *et al*., 1995; Goldberg *et al*., 2004; Weber *et al*., 2004).

RESULTS

ERp29 Depletion Disrupts Cx43 Trafficking and Function

To assess whether ERp29 may have a role in regulating Cx43 trafficking, we tested ERp29-specific siRNA oligonucleotides on three different cell models: ROS cells and human lung epithelial (A549) cells, both expressing endogenous Cx43, and HeLa cells expressing transfected Cx43 (HeLa/Cx43). Under the conditions we used, siRNA treatment reduced ERp29 protein expression by 58 ± 9% (n = 5) for ROS cells and 76 ± 11% (n = 5) for HeLa/Cx43 cells as determined by immunoblot (see Figure 4). By immunofluorescence microscopy, siRNA knockdown of ERp29 in both ROS and HeLa/Cx43 cells decreased gap junction plaque formation by Cx43 (Figure 1, B, H, and J) The correlation between ERp29 knockdown and disruption of Cx43 trafficking was further confirmed by examining cells double labeled for ERp29 and Cx43 by immunofluorescence microscopy (Supplemental Figure S2). A similar effect was observed for A549 cells (Supplemental Figure S3). By contrast, cells treated with control siRNA showed little effect on Cx43 trafficking (Figure 1, C and I). The effect of ERp29 depletion on Cx43 trafficking was confirmed using two different specific siRNAs targeting ERp29, which produced similar effects (Figure 1J). Also, transport of another class of tetraspan junction protein, claudin-4, was not affected by ERp29 depletion, suggesting that ERp29 depletion did not cause a generalized disruption of transmembrane protein trafficking (Figure 1E).

Cx43 accumulated inside the cells when ERp29 was depleted. The intracellular pool of Cx43 in ERp29-depleted

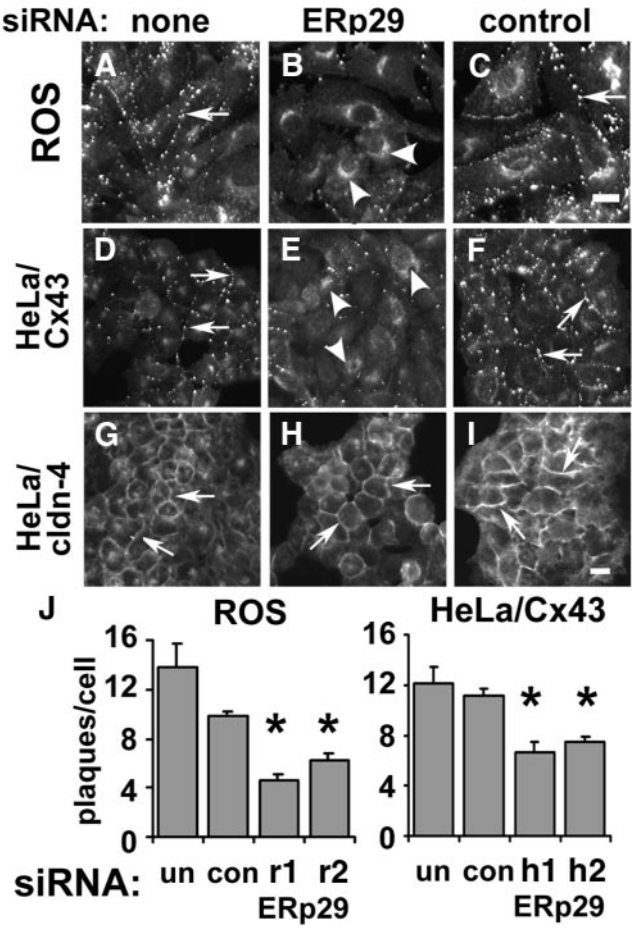

Figure 1. ERp29 depletion interferes with Cx43 trafficking to the plasma membrane. ROS (A–C), HeLa/Cx43 (D–F) or HeLa/cldn-4 (G–I) cells were either untreated (A, D, and G), transfected with ERp29 siRNA (B, E, and H) or with control siRNA (C, F, and I), and further incubated for 48 h. The cells were then fixed and immunostained for either Cx43 (A–F) or claudin-4 (G–I). Both untreated and control cells showed Cx43 present at cell–cell interfaces with a distribution consistent with gap junction plaque formation (arrows). However, 48 h after treatment with ERp29 siRNA, surface labeling of Cx43 was diminished and instead accumulated in the perinuclear region of the cell (arrowheads). In contrast to Cx43, a tight junction protein, claudin-4, remained plasma membrane localized (arrows), even in cells treated with ERp29 siRNA. Bar, 10 μm. (J) Gap junction plaques at intercellular junctions were quantified by image analysis for ROS and HeLa/Cx43 cells that were either untreated (un), treated with control siRNA (con), or two different target-specific ERp29 siRNAs specific for rat ERp29 (r1, r2) or human ERp29 (h1, h2). ERp29 depletion decreased the average number of gap junction plaques/cell (*$p < 0.05$ vs. control-treated cells).

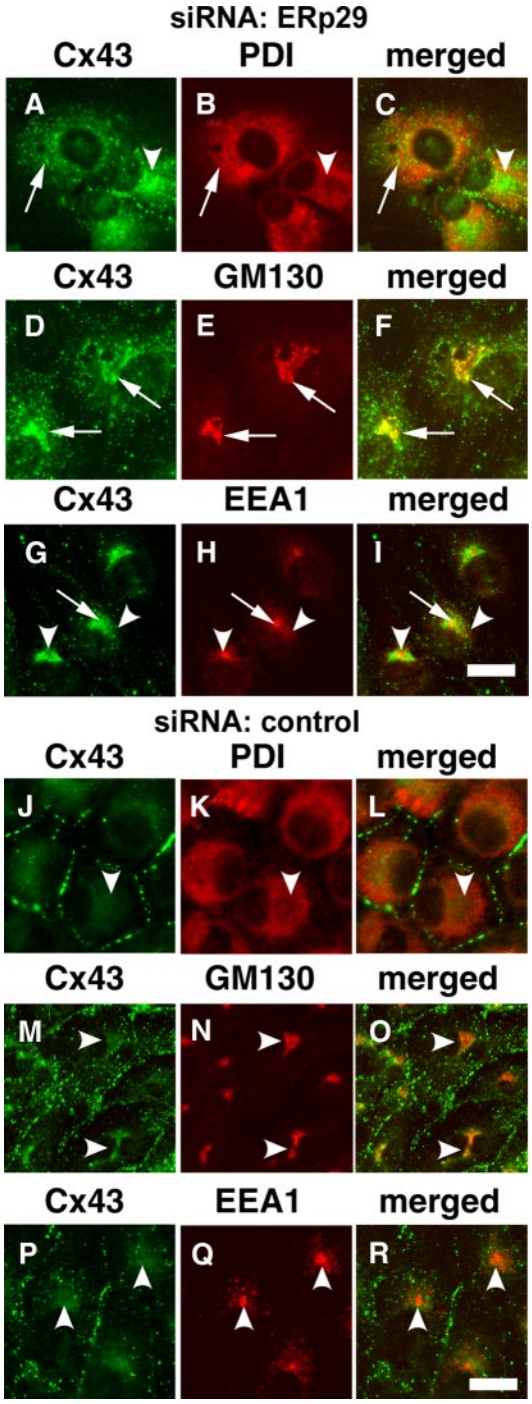

Figure 2. Intracellular Cx43 localized predominantly to the Golgi apparatus in ERp29-depleted cells. ROS cells were transfected with either ERp29 siRNA (A–I) or with control siRNA (J–R) and further incubated for 48 h. The cells were then fixed and immunostained for Cx43 (A, D, G, J, M, and P) and an ER marker (PDI) (B and K), *cis*-Golgi marker (GM130) (E and K), or early endosome-associated protein 1 (EEA1) (H and Q). Merged images are in C, F, I, L, O, and R. In cells treated with ERp29 siRNA, Cx43 was retained in an intracellular compartment (arrowheads) that colocalized predominantly with GM130 (G–I). To a lesser extent, Cx43 also colocalized with PDI, in cells treated with ERp29 siRNA. (C) Colocalization between Cx43 and EEA1 was limited (I). Cells treated with control siRNA showed less intracellular Cx43. Bar, 10 μm.

ROS cells was predominantly localized to the Golgi apparatus based on immunofluorescence colocalization with a *cis*-Golgi marker, GM130 (Figure 2, D and F). Cx43 also localized to the Golgi apparatus of ERp29-depleted A549 cells and colocalized with mannosidase II (Supplemental Figure S4). To a lesser extent, ERp29-depleted cells had some Cx43

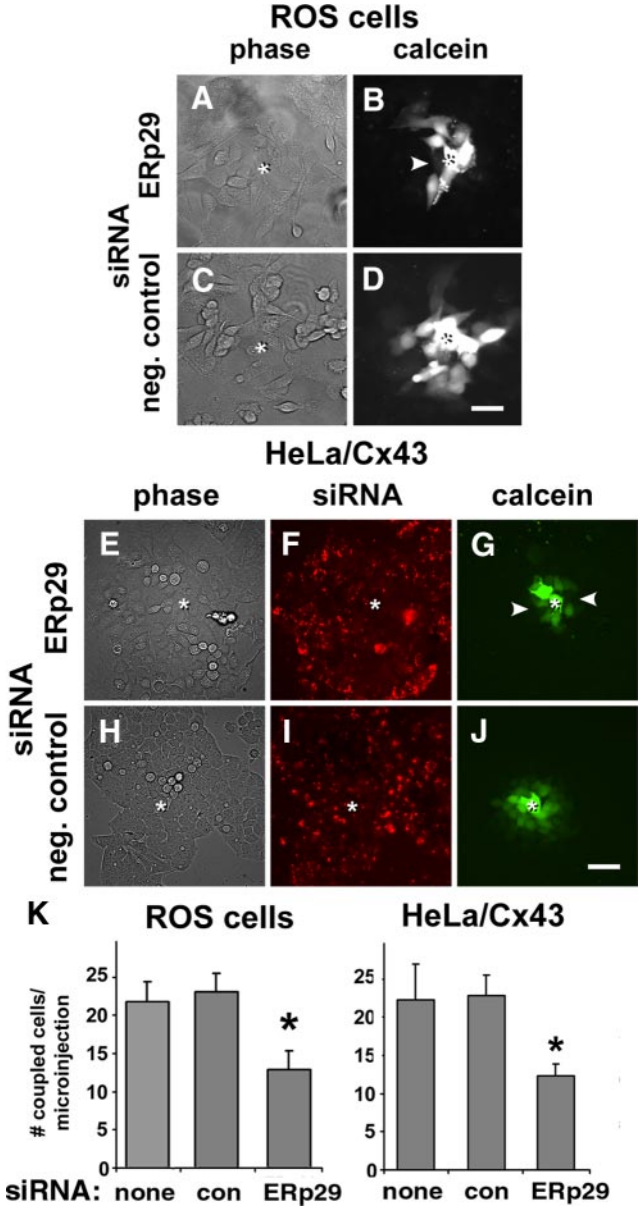

Figure 3. ERp29 depletion interferes with gap junctional communication. ROS (A–D) or HeLa/Cx43 cells (E–J) were transfected with ERp29 siRNA (A, B, and E–G) or control siRNA (C, D, and H–J) and then further incubated for 48 h. For HeLa/Cx43 cells, the siRNA was labeled with Cy3 (F and I). Gap junctional communication was assessed by measuring the intercellular transfer of microinjected calcein. The injected cell is denoted by asterisk (*). Note that diffusion of microinjected dye was uniform for control cells; however, it was uneven for cells treated with ERp29, where arrowheads denote uncoupled cells (B and G). Bar, 50 μm. K. For each condition, cell coupling was scored as the number of calcein labeled cells per microinjection. Data show the average ± SE of 15–20 microinjections, performed on two independent preparations each. Cells treated with ERp29 siRNA showed decreased dye transfer compared with untreated and control siRNA-treated cells (*$p < 0.01$).

retained in the ER, as determined by colocalization with PDI (Figure 2, A–C, and Supplemental Figure S4), suggesting that Cx43 trafficking was impaired when ERp29 was depleted. There was also a small amount of Cx43 accumulation in early endosomes by ERp29-depleted ROS cells, as determined by colocalization with EEA1, indicating that a portion of the intracellular pool of Cx43 in ERp29-depleted cells was because of endocytosed Cx43 (Figure 2, B and H).

A decrease in gap junction plaque formation induced by ERp29 depletion is expected to decrease gap junctional communication. To test this hypothesis, the effect of ERp29 siRNA on intercellular dye transfer was measured (Figure 3). Treatment of ROS cells decreased intercellular transfer of microinjected calcein to adjacent cells by 57.0 ± 7.1% (n = 20) compared with cells treated with control siRNA. ERp29 depletion had a similar effect on Cx43/HeLa cells, where gap junctional coupling was reduced to 46.2 ± 8.1% (n = 15). Control siRNA and untreated cells showed comparable levels of gap junctional coupling. Taken together, these results imply that ERp29 was required for optimal formation of gap junctions by Cx43.

For ROS and A549 cells, the decrease in gap junction formation induced by ERp29 depletion was because of a change in steady-state Cx43 expression (Figure 4 and Supplemental Figure S3). Moreover, ERp29 depletion of ROS cells did not have a significant effect on steady-state levels of three other ER resident chaperones: PDI, ERp57, and BiP. In contrast, ERp29-depleted HeLa/Cx43 cells had a modest 35 ± 15% (n = 7) decrease in steady-state Cx43 (Figure 4J). ERp29-depletion of HeLa/Cx43 cells did not significantly affect PDI, ERp57, and BiP (Figure 4), and we ruled out an effect of ERp29 depletion on Cx43 mRNA transcription by quantitative RT-PCR (Supplemental Figure S5). Instead, the reduction in Cx43 was linked to a more rapid rate of Cx43 turnover. The $t_{1/2}$ for Cx43 turnover in ERp29-depleted cells was 2.2 ± 0.5 h compared with control siRNA-

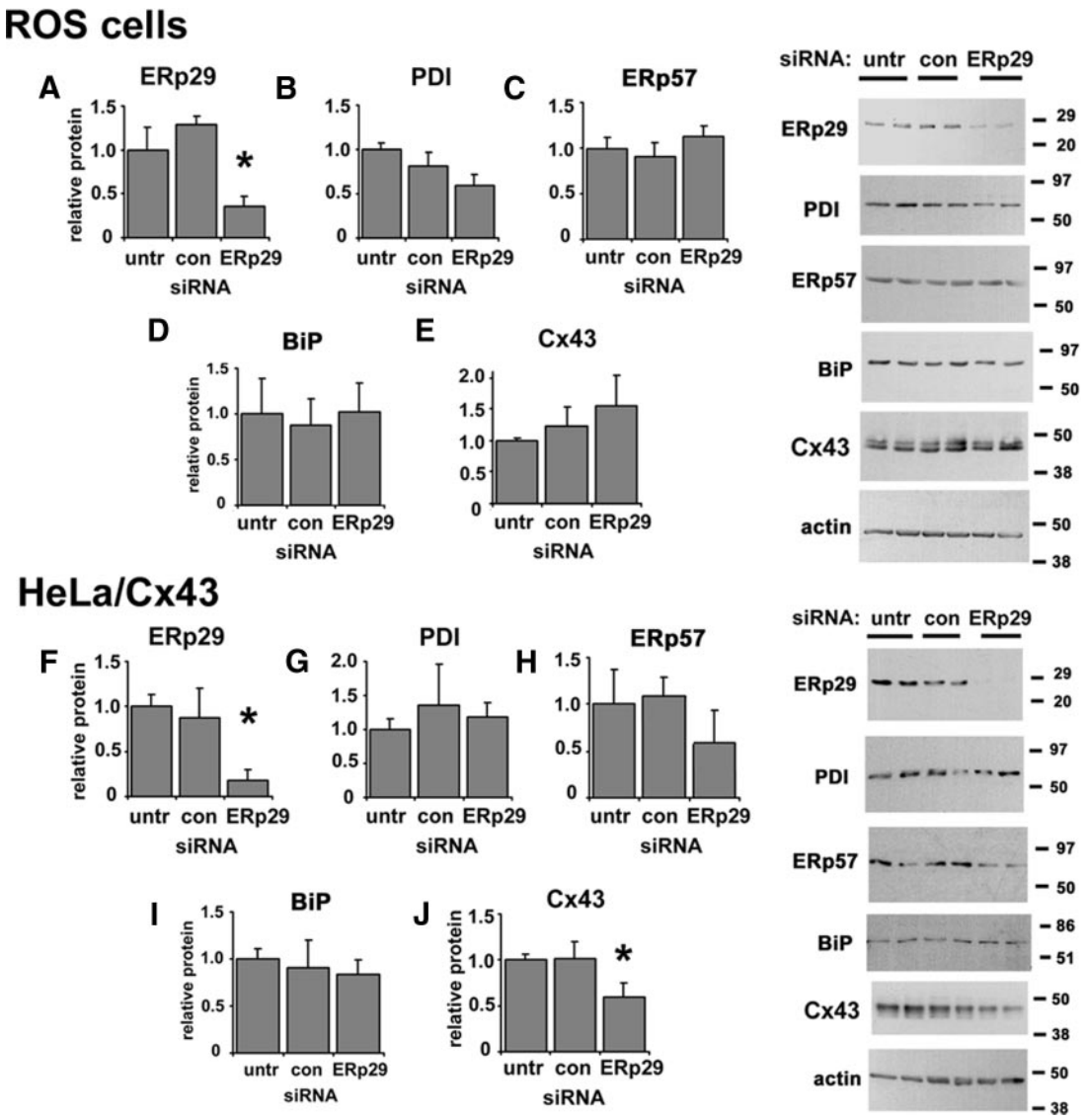

Figure 4. Depletion of ERp29 by siRNA. ROS (A–E) or HeLa/Cx43 (F–J) cells were either untreated or transfected with control or ERp29 siRNA. After 48 h, cells were harvested, homogenized, and postnuclear supernatants were resolved by reducing SDS-PAGE, transferred to Immobilon membranes, and immunoblotted for ERp29 (A and F), PDI (B and G), ERp57 (C and H), BiP (D and I), and Cx43 (E and J). As expected, Cx43 migrated as a doublet, reflecting multiple phosphorylation states of the protein. Parallel samples were immunoblotted to normalize for total protein and calculated as mean ± SE. *$p < 0.05$ (n = 5), significantly less than control treated cells.

treated cells, in which the $t_{1/2}$ value was 4.0 ± 0.4 h ($p < 0.05$) (Supplemental Figure S5). Treatment for 4 h with the proteosome inhibitor lactacystin (10 μM) increased the Cx43 content of ERp29-depleted HeLa/Cx43 cells to levels comparable with untransfected and control siRNA-treated cells, which suggests that ERp29 depletion increased the extent of proteosomal degradation of Cx43 by HeLa/Cx43 cells.

Effect of Normal and Mutant ERp29 on Cx43

To complement results obtained with siRNA, we used ERp29 constructs that were based on a strategy developed by Magnuson *et al*. (2005). A tagged form of ERp29 was produced by inserting an EGFP tag between the signal sequence and the N terminus of the mature ERp29 peptide (EGFP-ERp29, Supplemental Figure S1), to preserve the C-terminal KEEL ER retention/retrieval sequence (Demmer *et al*., 1997). EGFP-ERp29 was further mutated by deleting the C-terminal ligand binding domain (Magnuson *et al*., 2005; Barak *et al*., 2009; Rainey-Barger *et al*., 2009) while retaining the N-terminal dimerization domain and KEEL ER retention motif (EGFP-ERp29-N). As shown in Figure 5, cells expressing EGFP-ERp29 continued to form gap junctions containing Cx43. In contrast, expression of EGFP-ERp29-N disrupted transport of Cx43 to the plasma membrane (Figure 5B), comparable with the effect observed in cells in which ERp29 was depleted using siRNA (Figure 1).

We then examined the effect of EGFP-ERp29 and EGFP-ERp29-N on gap junctional communication by measuring the intercellular transfer of a red fluorescent dye, Alexa568, which does not overlap with the signal from EGFP-tagged proteins. Expression of EGFP-ERp29 did not change the level of gap junctional communication compared with control, untreated cells. However, cells transfected with EGFP-ERp29-N showed decreased gap junctional communication, in which intercellular transfer of Alexa568 was decreased by 42.6 ± 10.5% ($n = 15$; $p < 0.05$) compared with EGFP-transfected controls (Figure 5D). The ability of EGFP-ERp29-N to inhibit gap junctional communication was comparable with results obtained using siRNA to decrease ERp29 expression (Figure 2). EGFP-ERp29-N did not have a significant effect on PDI, ERp57, BiP, or Cx43 expression (Supplemental Figure S6), suggesting that the construct did not induce a generalized cell stress response. This provides further support for ERp29 as a key regulator for Cx43-mediated gap junctional communication.

The oxidant pesticide lindane inhibits Cx43 trafficking and gap junctional communication, in which lindane-treated cells resemble ERp29-depleted cells (Defamie *et al*., 2001; Loch-Caruso *et al*., 2004). Thus, we tested whether lindane had an effect on Cx43 and ERp29. Lindane treatment of ROS cells reduced Cx43 expression, transport of Cx43 to the plasma membrane, and intercellular communication in a dose-dependent manner (Figure 6, A–C). Moreover, lindane-treated ROS cells also had a dose-dependent decrease in ERp29 and Cx43 expression (Figure 6, D and E). Given this decrease in ERp29 expression, we tested whether overexpression of EGFP-ERp29 could protect ROS cells from the effects of lindane treatment on Cx43, which we found to be the case (Figure 6). ROS cells transfected with EGFP-ERp29 before lindane treatment expressed 3.1 ± 0.4-fold ($n = 4$) more Cx43 (Figure 6G) than untransfected, lindane-treated control cells (Figure 6E). The level of endogenous ERp29 was also protected from the effects of lindane by EGFP-ERp29, most likely because of heterodimer formation between ERp29 and EGFP-ERp29. Gap junctional intercellular communication (Figure 6U) was also significantly higher for lindane-treated ROS cells expressing EGFP-ERp29 compared with untransfected, lindane-treated controls. However, increased EGFP-ERp29 expression only partially rescued lindane-treated ROS cells, probably because of other toxic effects of lindane unrelated to ERp29 expression or function.

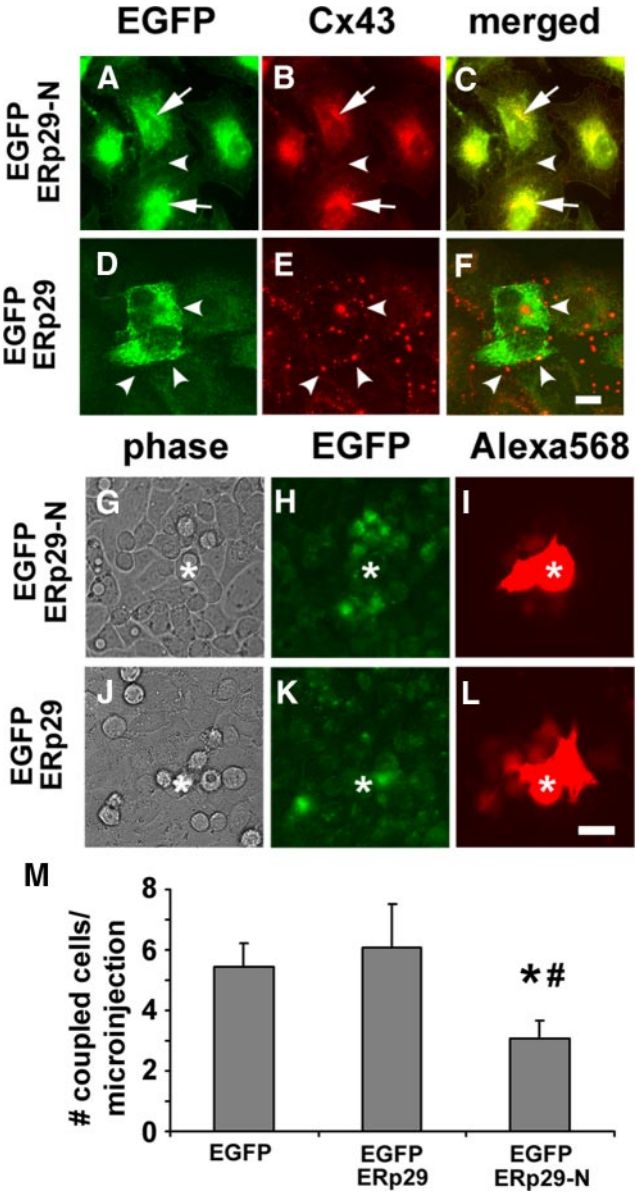

Figure 5. Truncated ERp29 inhibits Cx43-mediated gap junctional communication. (A–F) HeLa/Cx43 cells were transfected with either the N-terminal half of EGFP-ERp29 (EGFP-ERp29-N; A–C) or EGFP-ERp29 (D–F) and then fixed, permeabilized, and immunolabeled. Cells expressing EGFP-ERp29 showed accumulation of Cx43 inside the cells (arrows). In contrast, untransfected cells and cells transfected with EGFP-ERp29 had Cx43 localized to gap junctions (arrowheads). Bar, 10 μm. (G–L) Cells transfected with either EGFP-ERp29-N (G–I) or EGFP-ERp29 (J–L) were imaged, and gap junctional communication was assessed by measuring the intercellular transfer of microinjected Alexa568. The microinjected cell is denoted by asterisk (*). Data show the average ± SE of at least 15 microinjections, performed on two independent preparations each. Cells expressing EGFP-ERp29-N showed decreased dye transfer compared with cells expressing EGFP alone (*$p < 0.05$) and EGFP-ERp29 (#$p < 0.05$).

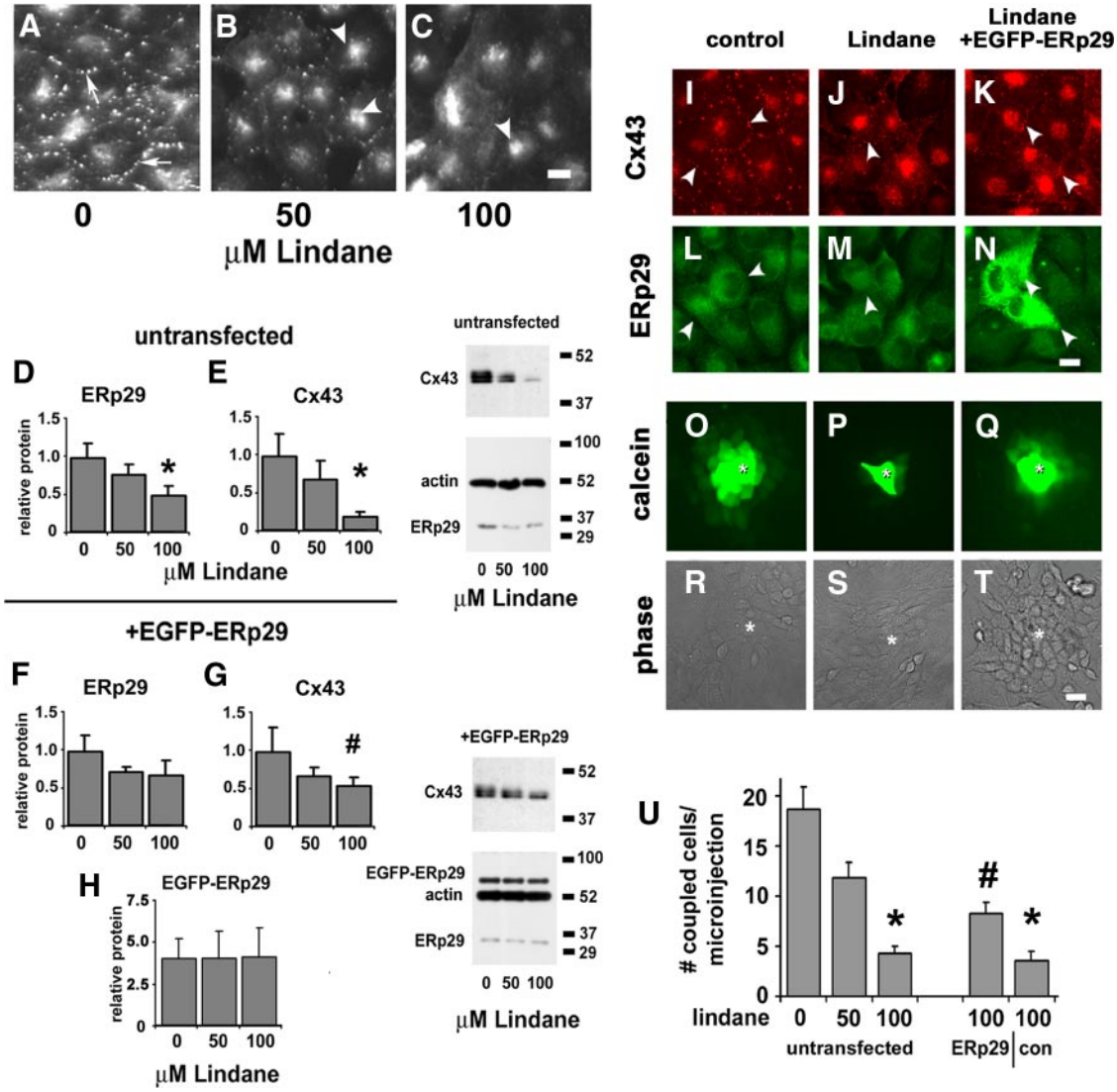

Figure 6. ERp29 prevents lindane-induced decreases in Cx43 expression, assembly, and gap junctional communication. (A–C) ROS cells were treated with 0 (A), 50 (B), or 100 μM lindane (C) for 16 h and then fixed, permeabilized, and immunolabeled for Cx43. With increasing lindane treatment, there was an increase in the relative amount of Cx43 localized to the perinuclear region of the cell (arrowheads) and a decrease in punctate gap junctional labeling. Bar, 10 μm. (D and E) ROS cells were treated with 0, 50, or 100 μM lindane for 16 h and then harvested and analyzed by immunoblot for ERp29 (D) and Cx43 (E) expression, normalized to actin expression. Asterisk (*), significantly less than control treated cells ($p < 0.05$; $n = 7$). (F–H) ROS cells were transfected with EGFP-ERp29 2 d before treatment with lindane as described above. Overexpression of EGFP-ERp29 partially prevented the decrease in Cx43 expression at 100 μM lindane (G) compared with untransfected cells (E) (#$p < 0.01$, $n = 4$). (I–N) Untransfected, control ROS cells immunolabeled for Cx43 (I) and ERp29 (L) show Cx43 localized to gap junction plaques at the cell surface (arrowheads). Transfection of ROS cells with EGFP-ERp29 before lindane treatment retained gap junction-localized Cx43 (K) in cells overexpressing EGFP-ERp29 (N). Bar, 10 μm. (O–U) Untransfected, control ROS cells show high levels of intercellular communication, as assessed by measuring the intercellular transfer of microinjected calcein (O). The injected cell is denoted by asterisk (*). Untransfected ROS cells treated for 16h with 100 μM lindane showed a decrease in gap junctional communication (P); however, cells transfected with EGFP-ERp29 before lindane treatment retained gap junctional communication (Q). Bar, 10 μm. (U) For each condition, cell coupling was scored as the number of calcein labeled cells per microinjection. Data show the average ± SE of at least 24 microinjections performed on three independent preparations each. Cells that were either untransfected or transfected with EGFP alone showed a significant decrease in gap junctional communication, compared with untreated controls (*$p < 0.01$). By contrast, ROS cells transfected with EGFP-ERp29 were resistant to Lindane and had increased gap junctional communication, as compared with control cells transfected with EGFP alone (#$p < 0.02$).

ERp29 Regulates Cx43 Oligomerization

These results supported a role for ERp29 as a chaperone to facilitate Cx43 trafficking. Cx43 processing is unique in that it oligomerizes into hexameric hemichannels in the Golgi apparatus as opposed to the ER (Koval, 2006). Thus, we hypothesized that ERp29 regulates Cx43 oligomerization by stabilizing monomeric Cx43 in the ER. To measure connexin oligomerization, we used blue native gel electrophoresis to resolve connexin monomers from oligomers (Figure 7). Cx43 expressed by NIH 3T3 cells, HeLa/Cx43 cells, and ROS cells resolved predominantly as two major fractions that migrated with sizes corresponding to monomeric and oligomerized Cx43, where the relative amount of Cx43 in the two fractions varied with cell type. This was consistent with

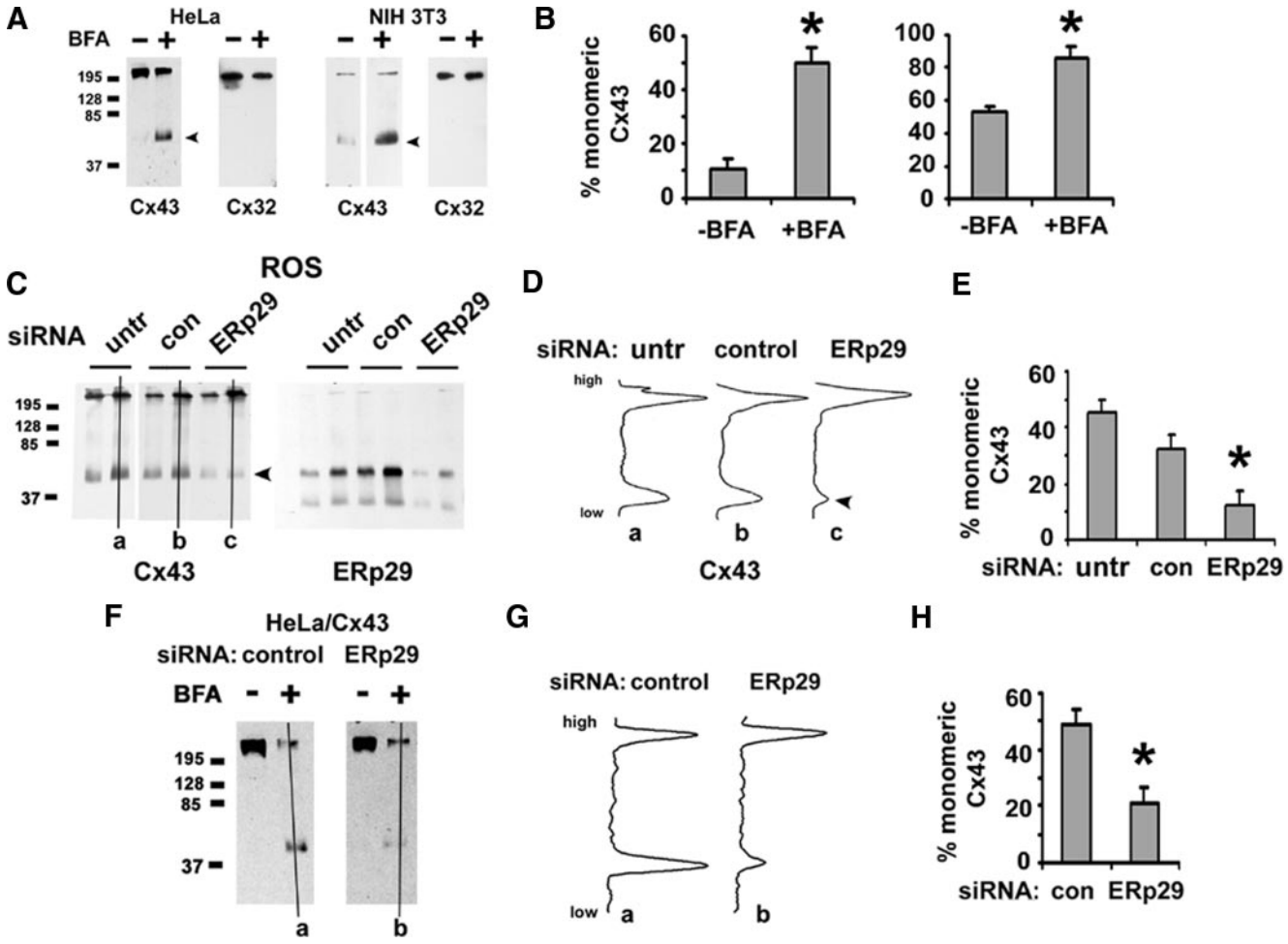

Figure 7. ERp29 depletion promotes early oligomerization of Cx43. (A and B) Blue native analysis of HeLa/Cx43, HeLa/Cx32 or NIH 3T3 cells that were either untreated (−) or incubated for 5 h with 6 μg/ml BFA (+), harvested, solubilized in 0.1% Triton X-100, resolved by blue native gel electrophoresis, and then transferred to immobilon membranes. Cx32 and Cx43 were visualized by immunoblot. (B) Note that BFA significantly increased the percentage of monomeric Cx43 (*$p < 0.05$; $n = 3$), in contrast to Cx32, which is not sensitive to BFA. (C–E) ROS cells were either untreated, or treated with control siRNA or ERp29 siRNA for 48 h and then harvested and further analyzed by blue native gel electrophoresis and immunoblot for Cx43 and ERp29. Note the ERp29 band that comigrated with monomeric Cx43. (D) Line scans from representative gels (a–c) in C show that ERp29 depletion decreased the amount of monomeric Cx43 (arrowhead), which was also quantified in E (*$p < 0.05$; $n = 3$). (F–H) HeLa/Cx43 cells were treated with control or ERp29 siRNA for 48 h and then further incubated for 5 h in either the absence (−) or presence (+) of BFA, and the oligomerization state of Cx43 was analyzed by blue native gel electrophoresis. (G) Line scans for samples treated with BFA (a and b) in F show that in cells in which ERp29 was depleted, the ability of BFA to promote the retention of monomeric Cx43 was diminished (H) (*$p < 0.05$; $n = 3$) compared with control cells, suggesting a role for ERp29 in limiting Cx43 oligomerization in the ER.

previous analysis of Cx43 oligomerization by using other approaches (Musil and Goodenough, 1993; Das Sarma *et al*., 2002, 2005; Maza *et al*., 2005).

Because Cx43 oligomerization occurs after exit from the Golgi apparatus (Musil and Goodenough, 1993; Koval *et al*., 1997), we also pretreated cells with brefeldin A before processing to inhibit membrane traffic from the ER to the Golgi apparatus. As expected, brefeldin A enriched the amount of Cx43 in the monomer band (Figure 7, A and B). In contrast to Cx43, Cx32 migrated predominantly as a higher molecular weight complex, as determined using HeLa/Cx32 and 3T3 cells expressing transfected and endogenous Cx32, respectively. Because 3T3 cells simultaneously express endogenous Cx43 and Cx32, these cells were particularly useful as a control for blue native gel electrophoresis and the effects of brefeldin A on Cx43. Consistent with our previous results (Das Sarma *et al*., 2002), the migration pattern for Cx32 by blue native gel electrophoresis was insensitive to brefeldin A treatment, indicating Cx32 oligomerization occurred in the ER, distinct from Cx43.

We then examined the effect of ERp29 depletion on Cx43 oligomerization by ROS cells (Figure 7, C–E). After treatment with ERp29 siRNA, the amount of monomeric Cx43 substantially decreased compared with untreated ROS cells and cells treated with control siRNA (Figure 7, B and C). To further explore the effect of ERp29 depletion on Cx43 oligomerization, HeLa/Cx43 cells were first treated with ERp29 siRNA and then further treated with brefeldin A to retain Cx43 in the ER (Figure 7, F–H). In contrast to HeLa/Cx43 cells expressing normal levels of ERp29, ERp29-depleted cells treated with brefeldin A showed less monomeric Cx43 than control-transfected cells, as expected if ERp29 is required to stabilize monomeric Cx43 in the ER. Combined with the observation that ERp29-

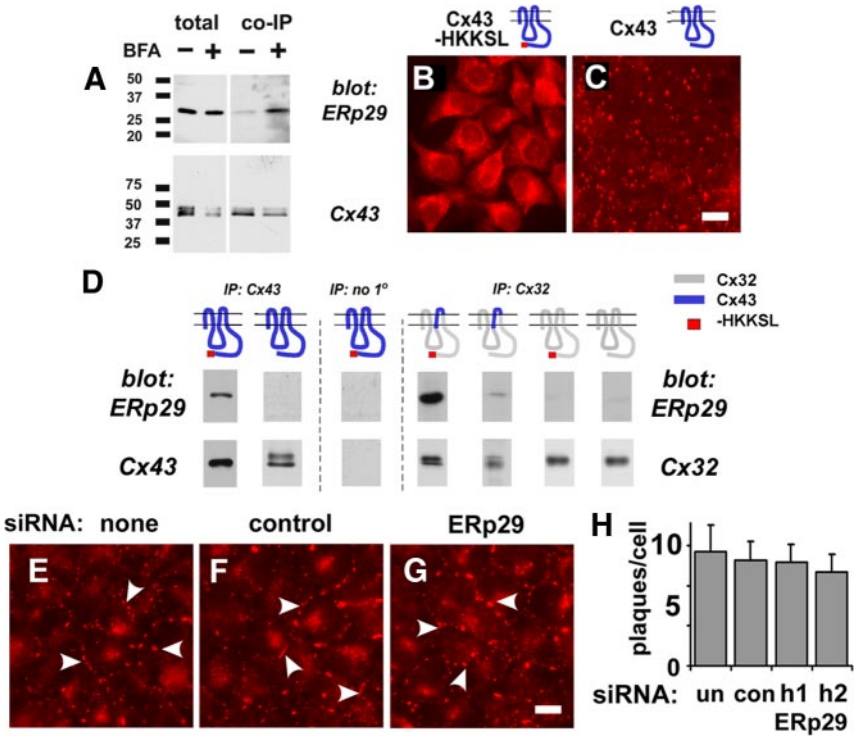

Figure 8. ERp29 forms a complex with Cx43. (A) HeLa/Cx43 cells were either untreated (−) or incubated for 5 h with 6 μg/ml BFA (+). The cells were then harvested, solubilized in 0.1% Triton X-100, and magnetically immunopurified with mouse anti-Cx43 and anti-mouse IgG BioMags, resolved by SDS-PAGE, and immunoblotted with rabbit anti-ERp29 or rabbit anti-Cx43. ERp29 preferentially coimmunopurified with Cx43 isolated from BFA-treated cells, suggesting an enhanced interaction when Cx43 is retained in the ER. (B and C) Immunolabeled HeLa shows retention of Cx43-HKKSL in the ER (B), whereas cells expressing wild-type Cx43 show localization to gap junctions (C). Bar, 10 μm. (D) Cells expressing different connexin constructs were homogenized, processed, and immunopurified as described above. ERp29 preferentially coimmunopurified with constructs that were predominantly monomeric (Cx43-HKKSL and Cx32/43/32-HKKSL), but not Cx32-HKKSL, which is oligomerized (Maza *et al*., 2005). Control samples processed in the absence of mouse anti-Cx43 showed no interaction with ERp29. (E–H) HeLa/Cx32 cells were either untreated (E) or transfected with ERp29 siRNA (F) or with control siRNA (G) and further incubated for 48 h. The cells were then fixed and immunostained for Cx32, which was quantified as number of plaques per cell (H).

depleted cells showed decreased Cx43 transport to the plasma membrane (Figure 1), these results imply that premature oligomerization of Cx43 impedes efficient trafficking along the secretory pathway.

Formation of a Specific Complex between ERp29 and Cx43

Some ERp29 comigrated with Cx43 in blue native gels, which may reflect formation of a complex between containing these two proteins (Figure 7B). To test this hypothesis, we performed coimmunopurification experiments from cell extracts solubilized in 0.1% Triton X-100. HeLa/Cx43 cells treated with brefeldin A to prevent Cx43 efflux from the ER showed that Cx43 and ERp29 were in a stable complex, because ERp29 coimmunopurified with Cx43 (Figure 8A). By contrast, in untreated cells the amount of ERp29 associated with Cx43 was less prominent, correlating ERp29 binding, ER localization of Cx43 and stabilization of monomeric Cx43.

We previously developed a series of connexin constructs containing an ER retention/retrieval motif, to study early events in connexin oligomerization without requiring agents such as brefeldin A (Das Sarma *et al*., 2002, 2005; Maza *et al*., 2005). Expression of this construct produces a population of cells containing only an ER-localized form of Cx43 (Figure 8, B and C). By coimmunopurification (Figure 8D), ERp29 preferentially interacted with ER-retained Cx43-HKKSL as opposed to untagged Cx43, consistent with results obtained using brefeldin A. In parallel experiments, we were unable to detect a stable complex of Cx43-HKKSL containing either PDI, ERp57, or BiP under these conditions (unpublished data). These results further strengthen the argument that ERp29 has a role in stabilizing monomeric Cx43. Whether ERp29 binds directly to Cx43 or is part of a larger complex requiring other protein cofactors is not known at present.

We further explored the specificity of ERp29–Cx43 interactions by using two previously described HKKSL-tagged constructs: Cx32-HKKSL and a chimeric Cx32/43/32-HKKSL construct that contain the third transmembrane (TM3) domain and second extracellular loop (EL2) domain of Cx43 on a Cx32 backbone (Das Sarma *et al*., 2002; Maza *et al*., 2005). We previously found that Cx32-HKKSL oligomerizes in the ER, whereas Cx32/43/32-HKKSL contains the minimal Cx43 motif required to be stabilized in the ER as a monomer (Maza *et al*., 2005). As shown in Figure 8D, ERp29 coimmunopurified with Cx32/43/32-HKKSL but not Cx32-HKKSL, indicating that the EL2 domain of Cx43 in the ER lumen is required for an interaction with ERp29.

ERp29 only coimmunopurified with connexin constructs that were stabilized as monomers in the ER (Das Sarma *et al*., 2002; Maza *et al*., 2005). In fact, ERp29 had, at most, a weak interaction with Cx32-HKKSL. Based on this result, we predicted that ERp29 depletion would have little effect on the transport and assembly of Cx32 into gap junction plaques. As shown in Figure 8, E–H, HeLa/Cx32 cells that were either untreated, treated with control siRNA or ERp29 siRNA showed comparable levels of gap junction plaque assembly. Thus, Cx32 was not regulated by ERp29, consistent with differential interactions between ERp29 and different classes of connexins.

DISCUSSION

We found that an ER-associated protein, ERp29, regulated Cx43 trafficking and assembly into gap junctions. Critically, ERp29 stabilized monomeric Cx43 in the ER by forming a stable complex with Cx43 (Figure 9). ERp29-depletion decreased the level of monomeric Cx43, caused Cx43 to accumulate in the early secretory pathway and decreased the number of functional gap junction channels. Thus, the ERp29–Cx43 complex facilitates the exit of monomeric Cx43 from the ER to sites of oligomerization in the *trans*-Golgi apparatus (TGN) (Musil and Goodenough, 1993; Koval *et al*., 1997).

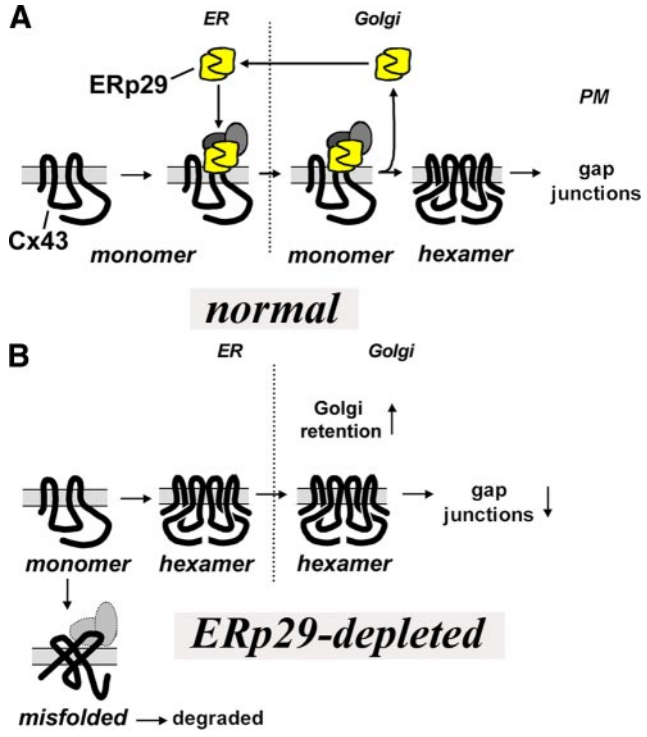

Figure 9. Model for ERp29/Cx43 interactions. ERp29 binding to one or both of the EL domains helps stabilize monomeric Cx43. On exit from the ER to the Golgi apparatus, ERp29 dissociation allows Cx43 oligomerization, presumably by allowing an conformational shift in Cx43. Here, the hexamers are represented by two of the six connexins in the oligomeric complex. The possibility that other protein cofactors may also be part of the ERp29–connexin complex is indicated by the gray circles. In the absence of ERp29, Cx43 prematurely oligomerizes, which increases retention in the Golgi apparatus, increases the potential for Cx43 misfolding/degradation and decreases gap junction formation.

In contrast to Cx43, Cx32 did not interact with ERp29 (Figure 8). This difference in binding capacity correlated with the ability of Cx32 to oligomerize in the ER as opposed to Cx43, which oligomerizes in the TGN (Figure 7A), results that further support a role for ERp29 in stabilizing connexin monomers. Interestingly, Cx43 is a member of the α subclass of connexins, whereas Cx32 is a β connexin (Willecke *et al.*, 1991), suggesting the possibility that the range of interaction for ERp29 is limited to a subset of connexins. Connexin oligomerization is a regulated process, and cells have the capacity to restrict formation of heteromeric channels by biochemically compatible connexins (Koval, 2006). Thus, the finding that ERp29 has differential interactions with different connexins suggests that it is an intriguing candidate chaperone to regulate hetero-oligomerization. Defining the range and affinity of interaction between ERp29 for different connexins is required to determine whether ERp29 regulates heteromer formation involving different connexins.

Mice deficient in Cx46, an α connexin, develop more severe cataracts on a 129/SvJ background than Cx46-deficiency on a C57BL/6J background (Gong *et al.*, 1999). A recent proteomic screen determined that one of the differences between these strains is that the lenses of 129/SvJ mice have significantly less ERp29 than lenses of C57BL//6J mice (Hoehenwarter *et al.*, 2008). Cx46-deficient lenses do contain other connexins that continue to be assembled into gap junctions, most notably Cx50, another α connexin (Gong *et al.*, 1997; White *et al.*, 1998). Thus, it is tempting to speculate that the increased severity of cataract in 129/SvJ mice may reflect decreased assembly of Cx50 into gap junctions because of a lack ERp29. In addition to null mutations leading to connexin deficiency, there are several disease-causing connexin mutations leading to structural changes that impede connexin transport to the plasma membrane (Shibayama *et al.*, 2005; Orthmann-Murphy *et al.*, 2007; Laird, 2008). Our findings that ERp29 interacts with normal Cx43 suggests that mutations that disrupt ERp29–connexin interactions would be expected to impair connexin trafficking.

We found that ERp29 depletion increased the rate of Cx43 turnover by HeLa/Cx43 cells resulting in decreased steady-state levels of Cx43 (Figure 5). The decrease in Cx43 was antagonized by lactacystin, suggesting that ERp29 depletion increased proteosomal degradation of Cx43. Because retrotranslocation of connexins out of the ER is linked to ERAD (VanSlyke and Musil, 2002), this finding seems in apparent contradiction with the critical role for ERp29 in unfolding and ER retrotranslocation of the polyomavirus VP1 protein (Magnuson *et al.*, 2005; Rainey-Barger *et al.*, 2009). However, it seems likely that ERp29 plays different roles in regulating retrotranslocation and secretion. Consistent with this possibility, point mutants in the C-terminal domain of ERp29 which interfered with VP1 binding and retrotranslocation retained the capacity to stimulate thyroglobulin secretion (Magnuson *et al.*, 2005; Rainey-Barger *et al.*, 2009). With respect to Cx43, ERp29 may not be required for retrotranslocation and instead could play a more prominent role in stabilizing Cx43 insertion into the ER membrane analogous to other chaperone proteins that perform a comparable function (Lyman and Schekman, 1997).

It is likely that a conformational change in Cx43 is required for oligomerization. Consistent with changes in Cx43 folding that can accompany transport along the secretory pathway, conformation specific antibodies against the C terminus of Cx43 have been identified that specifically recognize either Golgi- or gap junction-localized Cx43 (Sosinsky *et al.*, 2007). In particular, the fully formed connexin channel contains an aqueous pore lined by polar and charged amino acids from multiple connexin transmembrane domains (Yeager and Harris, 2007). Thus, the conformation Cx43 assumes when assembled into a hexamer is expected to be unstable for monomeric Cx43 because these polar residues would be exposed to the hydrophobic portion of the membrane instead of part of the aqueous pore. These observations suggest a model where the ERp29–Cx43 complex stabilizes monomeric Cx43 in an alternative conformation more favorably inserted in the membrane by shielding polar amino acids from the hydrophobic portion of the bilayer. Although there is limited information on the structure of monomeric connexins in the membrane, the transmembrane α helical domains of oligomerized connexins are significantly tilted relative to the plane of the bilayer (Fleishman *et al.*, 2004), consistent with the possibility that a change in transmembrane orientation may favor stable monomer insertion into the bilayer.

Connexins assembled into gap junction channels are stabilized by disulfide bonds between the EL domains (Rahman *et al.*, 1993; Foote *et al.*, 1998; Unger *et al.*, 1999; Bao *et al.*, 2004). Catalysis to form these disulfide bonds requires an enzyme with oxidase activity, such as one of the PDIs. Although PDI and ERp29 are both thioredoxin fold proteins, ERp29 lacks the Cys-X-X-Cys motif required to form disulfide bonds (Demmer *et al.*, 1997; Liepinsh *et al.*, 2001; Hubbard *et al.*, 2004; Mkrtchian and Sandalova, 2006). This characteristic of

ERp29 raises the intriguing possibility that ERp29 stabilizes the conformation of monomeric Cx43 by blocking cysteine oxidases from forming disulfide bonds between the EL domains. Although unable to catalyze formation of disulfide bonds, ERp29 has a cysteine residue that could participate in disulfide bond editing (Hubbard *et al*., 2004; Hermann *et al*., 2005; Baryshev *et al*., 2006). Thus, ERp29 could potentially have a role in rearranging mismatched disulfide bonds formed between the EL domains. Characterizing the binding sites for ERp29 and identifying the enzymes that catalyze the oxidation of connexin EL domains will enable us to further define the mode of action for ERp29 in regulating Cx43 and other connexins.

ACKNOWLEDGMENTS

This work was supported by National Institutes of Health grants GM-61012, HL-083120, AA-013757 (to M. K.), DK-58046 (to R.C.R.), and AA-013528 (to L.A.C.); the University Research Committee of Emory University (to M. K.); and the American Heart Association (to L. S.). R.C.R. was an Established Investigator of the American Heart Association. M. H. was supported by a Professorial Fellowship from the Melbourne Research Unit for Facial Disorders.

REFERENCES

Anelli, T., and Sitia, R. (2008). Protein quality control in the early secretory pathway. EMBO J. *27*, 315–327.

Asklund, T., Appelskog, I. B., Ammerpohl, O., Ekstrom, T. J., and Almqvist, P. M. (2004). Histone deacetylase inhibitor 4-phenylbutyrate modulates glial fibrillary acidic protein and connexin 43 expression, and enhances gap-junction communication, in human glioblastoma cells. Eur. J. Cancer *40*, 1073–1081.

Bao, X., Chen, Y., Reuss, L., and Altenberg, G. A. (2004). Functional expression in *Xenopus* oocytes of gap-junctional hemichannels formed by a cysteine-less connexin 43. J. Biol. Chem. *279*, 9689–9692.

Barak, N. N., Neumann, P., Sevvana, M., Schutkowski, M., Naumann, K., Malesevic, M., Reichardt, H., Fischer, G., Stubbs, M. T., and Ferrari, D. M. (2009). Crystal structure and functional analysis of the protein disulfide isomerase-related protein ERp29. J. Mol. Biol. *385*, 1630–1642.

Baryshev, M., Sargsyan, E., and Mkrtchian, S. (2006). ERp29 is an essential endoplasmic reticulum factor regulating secretion of thyroglobulin. Biochem. Biophys. Res. Commun. *340*, 617–624.

Berthoud, V. M., Minogue, P. J., Guo, J., Williamson, E. K., Xu, X., Ebihara, L., and Beyer, E. C. (2003). Loss of function and impaired degradation of a cataract-associated mutant connexin50. Eur. J. Cell Biol. *82*, 209–221.

Civitelli, R., Beyer, E. C., Warlow, P. M., Robertson, A. J., Geist, S. T., and Steinberg, T. H. (1993). Connexin43 mediates direct intercellular communication in human osteoblastic cell networks. J. Clin. Invest. *91*, 1888–1896.

Das Sarma, J., Das, S., and Koval, M. (2005). Regulation of connexin43 oligomerization is saturable. Cell Commun. Adhes. *12*, 237–247.

Das Sarma, J., Kaplan, B. E., Willemsen, D., and Koval, M. (2008). Identification of rab20 as a potential regulator of connexin43 trafficking. Cell Commun. Adhes. *15*, 65–74.

Das Sarma, J., Meyer, R. A., Wang, F., Abraham, V., Lo, C. W., and Koval, M. (2001). Multimeric connexin interactions prior to the trans-Golgi network. J. Cell Sci. *114*, 4013–4024.

Das Sarma, J., Wang, F., and Koval, M. (2002). Targeted gap junction protein constructs reveal connexin-specific differences in oligomerization. J. Biol. Chem. *277*, 20911–20918.

Daugherty, B. L., Ward, C., Smith, T., Ritzenthaler, J. D., and Koval, M. (2007). Regulation of heterotypic claudin compatibility. J. Biol. Chem. *282*, 30005–30013.

Defamie, N., Mograbi, B., Roger, C., Cronier, L., Malassine, A., Brucker-Davis, F., Fenichel, P., Segretain, D., and Pointis, G. (2001). Disruption of gap junctional intercellular communication by lindane is associated with aberrant localization of connexin43 and zonula occludens-1 in 42GPA9 Sertoli cells. Carcinogenesis *22*, 1537–1542.

Demmer, J., Zhou, C., and Hubbard, M. J. (1997). Molecular cloning of ERp29, a novel and widely expressed resident of the endoplasmic reticulum. FEBS Lett. *402*, 145–150.

Ellgaard, L., and Helenius, A. (2003). Quality control in the endoplasmic reticulum. Nat. Rev. Mol. Cell Biol. *4*, 181–191.

Fleishman, S. J., Unger, V. M., Yeager, M., and Ben-Tal, N. (2004). A C(alpha) model for the transmembrane alpha helices of gap junction intercellular channels. Mol Cell *15*, 879–888.

Foote, C. I., Zhou, L., Zhu, X., and Nicholson, B. J. (1998). The pattern of disulfide linkages in the extracellular loop regions of connexin 32 suggests a model for the docking interface of gap junctions. J. Cell Biol. *140*, 1187–1197.

Goldberg, G. S., Valiunas, V., and Brink, P. R. (2004). Selective permeability of gap junction channels. Biochim. Biophys. Acta *1662*, 96–101.

Gong, X., Agopian, K., Kumar, N. M., and Gilula, N. B. (1999). Genetic factors influence cataract formation in alpha 3 connexin knockout mice. Dev. Genet. *24*, 27–32.

Gong, X., Li, E., Klier, G., Huang, Q., Wu, Y., Lei, H., Kumar, N. M., Horwitz, J., and Gilula, N. B. (1997). Disruption of alpha3 connexin gene leads to proteolysis and cataractogenesis in mice. Cell *91*, 833–843.

Goodenough, D. A., and Paul, D. L. (2003). Beyond the gap: functions of unpaired connexon channels. Nat. Rev. Mol. Cell Biol. *4*, 285–294.

Harris, A. L. (2001). Emerging issues of connexin channels: biophysics fills the gap. Q. Rev. Biophys. *34*, 325–472.

Hermann, V. M., Cutfield, J. F., and Hubbard, M. J. (2005). Biophysical characterization of ERp29. Evidence for a key structural role of cysteine 125. J. Biol. Chem. *280*, 13529–13537.

Hoehenwarter, W., Tang, Y., Ackermann, R., Pleissner, K. P., Schmid, M., Stein, R., Zimny-Arndt, U., Kumar, N. M., and Jungblut, P. R. (2008). Identification of proteins that modify cataract of mouse eye lens. Proteomics *8*, 5011–5024.

Hubbard, M. J., Mangum, J. E., and McHugh, N. J. (2004). Purification and biochemical characterization of native ERp29 from rat liver. Biochem. J. *383*, 589–597.

Hubbard, M. J., and McHugh, N. J. (2000). Human ERp 29, isolation, primary structural characterisation and two-dimensional gel mapping. Electrophoresis *21*, 3785–3796.

Kelsell, D. P., Dunlop, J., and Hodgins, M. B. (2001). Human diseases: clues to cracking the connexin code? Trends Cell Biol. *11*, 2–6.

Khan, Z., Akhtar, M., Asklund, T., Juliusson, B., Almqvist, P. M., and Ekstrom, T. J. (2007). HDAC inhibition amplifies gap junction communication in neural progenitors: potential for cell-mediated enzyme prodrug therapy. Exp. Cell Res. *313*, 2958–2967.

Koval, M. (2006). Pathways and control of connexin oligomerization. Trends Cell Biol. *16*, 159–166.

Koval, M., Geist, S. T., Westphale, E. M., Kemendy, A. E., Civitelli, R., Beyer, E. C., and Steinberg, T. H. (1995). Transfected connexin45 alters gap junction permeability in cells expressing endogenous connexin43. J. Cell Biol. *130*, 987–995.

Koval, M., Harley, J. E., Hick, E., and Steinberg, T. H. (1997). Connexin46 is retained as monomers in a trans-Golgi compartment of osteoblastic cells. J. Cell Biol. *137*, 847–857.

Laird, D. W. (2006). Life cycle of connexins in health and disease. Biochem. J. *394*, 527–543.

Laird, D. W. (2008). Closing the gap on autosomal dominant connexin-26 and connexin-43 mutants linked to human disease. J. Biol. Chem. *283*, 2997–3001.

Liepinsh, E., Baryshev, M., Sharipo, A., Ingelman-Sundberg, M., Otting, G., and Mkrtchian, S. (2001). Thioredoxin fold as homodimerization module in the putative chaperone ERp *29*, NMR structures of the domains and experimental model of the 51 kDa dimer. Structure *9*, 457–471.

Loch-Caruso, R., Galvez, M. M., Brant, K., and Chung, D. (2004). Cell and toxicant specific phosphorylation of conexin *43*, effects of lindane and TPA on rat myometrial and WB-F344 liver cell gap junctions. Cell Biol. Toxicol. *20*, 147–169.

Lyman, S. K., and Schekman, R. (1997). Binding of secretory precursor polypeptides to a translocon subcomplex is regulated by BiP. Cell *88*, 85–96.

Ma, Q., Guo, C., Barnewitz, K., Sheldrick, G. M., Soling, H. D., Uson, I., and Ferrari, D. M. (2003). Crystal structure and functional analysis of *Drosophila* Wind, a protein-disulfide isomerase-related protein. J. Biol. Chem. *278*, 44600–44607.

Magnuson, B., Rainey, E. K., Benjamin, T., Baryshev, M., Mkrtchian, S., and Tsai, B. (2005). ERp29 triggers a conformational change in polyomavirus to stimulate membrane binding. Mol. Cell *20*, 289–300.

Martin, P. E., and Evans, W. H. (2004). Incorporation of connexins into plasma membranes and gap junctions. Cardiovasc. Res. *62*, 378–387.

Maza, J., Das Sarma, J., and Koval, M. (2005). Defining a minimal motif required to prevent connexin oligomerization in the endoplasmic reticulum. J. Biol. Chem. *280*, 21115–21121.

Maza, J., Mateescu, M., Das Sarma, J., and Koval, M. (2003). Differential oligomerization of endoplasmic reticulum-retained connexin43/connexin32 chimeras. Cell Commun. Adhes. *10*, 319–322.

Mkrtchian, S., and Sandalova, T. (2006). ERp29, an unusual redox-inactive member of the thioredoxin family. Antioxid. Redox Signal. *8*, 325–337.

Musil, L. S., and Goodenough, D. A. (1993). Multisubunit assembly of an integral plasma membrane channel protein, gap junction connexin43, occurs after exit from the ER. Cell *74*, 1065–1077.

Orthmann-Murphy, J. L., Enriquez, A. D., Abrams, C. K., and Scherer, S. S. (2007). Loss-of-function GJA12/Connexin47 mutations cause Pelizaeus-Merzbacher-like disease. Mol. Cell. Neurosci. *34*, 629–641.

Qin, H., Shao, Q., Igdoura, S. A., Alaoui-Jamali, M. A., and Laird, D. W. (2003). Lysosomal and proteasomal degradation play distinct roles in the life cycle of Cx43 in gap junctional intercellular communication-deficient and -competent breast tumor cells. J. Biol. Chem. *278*, 30005–30014.

Rahman, S., Carlile, G., and Evans, W. H. (1993). Assembly of hepatic gap junctions. Topography and distribution of connexin 32 in intracellular and plasma membranes determined using sequence-specific antibodies. J. Biol. Chem. *268*, 1260–1265.

Rainey-Barger, E. K., Mkrtchian, S., and Tsai, B. (2007). Dimerization of ERp29, a PDI-like protein, is essential for its diverse functions. Mol. Biol. Cell.

Rainey-Barger, E. K., Mkrtchian, S., and Tsai, B. (2009). The C-terminal domain of ERp29 mediates polyomavirus binding, unfolding, and infection. J. Virol. *83*, 1483–1491.

Rubenstein, R. C., Egan, M. E., and Zeitlin, P. L. (1997). In vitro pharmacologic restoration of CFTR-mediated chloride transport with sodium 4-phenylbutyrate in cystic fibrosis epithelial cells containing delta F508-CFTR. J. Clin. Invest. *100*, 2457–2465.

Rubenstein, R. C., and Zeitlin, P. L. (2000). Sodium 4-phenylbutyrate downregulates Hsc 70, implications for intracellular trafficking of DeltaF508-CFTR. Am. J. Physiol. Cell Physiol. *278*, C259–C267.

Saez, J. C., Berthoud, V. M., Branes, M. C., Martinez, A. D., and Beyer, E. C. (2003). Plasma membrane channels formed by connexins: their regulation and functions. Physiol. Rev. *83*, 1359–1400.

Sargsyan, E., Baryshev, M., Szekely, L., Sharipo, A., and Mkrtchian, S. (2002). Identification of ERp29, an endoplasmic reticulum lumenal protein, as a new member of the thyroglobulin folding complex. J. Biol. Chem. *277*, 17009–17015.

Schmittgen, T. D., Lee, E. J., Jiang, J., Sarkar, A., Yang, L., Elton, T. S., and Chen, C. (2008). Real-time PCR quantification of precursor and mature microRNA. Methods *44*, 31–38.

Segretain, D., and Falk, M. M. (2004). Regulation of connexin biosynthesis, assembly, gap junction formation, and removal. Biochim. Biophys. Acta *1662*, 3–21.

Shibayama, J., Paznekas, W., Seki, A., Taffet, S., Jabs, E. W., Delmar, M., and Musa, H. (2005). Functional characterization of connexin43 mutations found in patients with oculodentodigital dysplasia. Circ. Res. *96*, e83–91.

Sosinsky, G. E., Solan, J. L., Gaietta, G. M., Ngan, L., Lee, G. J., Mackey, M. R., and Lampe, P. D. (2007). The C-terminus of connexin43 adopts different conformations in the Golgi and gap junction as detected with structure-specific antibodies. Biochem. J. *408*, 375–385.

Suaud, L., Miller, K., Alvey, L., Yan, W., Robay, A., Hubbard, M., and Rubenstein, R. C. (2008). ERp *29*, A luminal chaperone that facilitates CFTR trafficking in response to 4-Phenylbutyrate. FASEB J. *22*, 1002.1002.

Unger, V. M., Kumar, N. M., Gilula, N. B., and Yeager, M. (1999). Three-dimensional structure of a recombinant gap junction membrane channel. Science *283*, 1176–1180.

VanSlyke, J. K., and Musil, L. S. (2002). Dislocation and degradation from the ER are regulated by cytosolic stress. J. Cell Biol. *157*, 381–394.

Wang, F., Daugherty, B., Keise, L. L., Wei, Z., Foley, J. P., Savani, R. C., and Koval, M. (2003). Heterogeneity of claudin expression by alveolar epithelial cells. Am. J. Respir. Cell. Mol. Biol. *29*, 62–70.

Weber, P. A., Chang, H. C., Spaeth, K. E., Nitsche, J. M., and Nicholson, B. J. (2004). The permeability of gap junction channels to probes of different size is dependent on connexin composition and permeant-pore affinities. Biophys. J. *87*, 958–973.

White, T. W., Goodenough, D. A., and Paul, D. L. (1998). Targeted ablation of connexin50 in mice results in microphthalmia and zonular pulverulent cataracts. J. Cell Biol. *143*, 815–825.

Willecke, K., Hennemann, H., Dahl, E., Jungbluth, S., and Heynkes, R. (1991). The diversity of connexin genes encoding gap junctional proteins. Eur. J. Cell Biol. *56*, 1–7.

Wittig, I., Braun, H. P., and Schagger, H. (2006). Blue native PAGE. Nat. Protoc. *1*, 418–428.

Wright, J. M., Zeitlin, P. L., Cebotaru, L., Guggino, S. E., and Guggino, W. B. (2004). Gene expression profile analysis of 4-phenylbutyrate treatment of IB3-1 bronchial epithelial cell line demonstrates a major influence on heat-shock proteins. Physiol. Genomics *16*, 204–211.

Yeager, M., and Harris, A. L. (2007). Gap junction channel structure in the early 21st century: facts and fantasies. Curr. Opin. Cell Biol. *19*, 521–528.